RSC Advances

PAPER

View Article Online
View Journal | View Issue

Cite this: *RSC Adv.*, 2014, **4**, 554

Synthesis, structure, photo- and electro-luminescence of an iridium(III) complex with a novel carbazole functionalized β-diketone ligand†

Tianzhi Yu,‡*[a] Yan Cao,‡[b] Wenming Su,[c] Chengcheng Zhang,[a] Yuling Zhao,[a] Duowang Fan,[a] Mingjun Huang,[b] Kan Yue[b] and Stephen Z. D. Cheng*[b]

A new iridium complex containing coumarin derivative as a cyclometalated ligand (^{1}L) and a carbazole-functionalized β-diketonate (^{2}L) as the ancillary ligand, namely, Ir(III)bis(3-(pyridin-2-yl)coumarinato-N,C^4)(1-(9-butyl-9*H*-carbazol-3-yl)-4,4,4-trifluoro-butane-1,3-dionato-*O*,*O*) (Ir(^{1}L)$_2$(^{2}L)), was synthesized. The crystal structure of Ir(^{1}L)$_2$(^{2}L) was determined *via* combined wide angle X-ray diffraction (WAXD) and transmission electron microscopy (TEM), which showed π–π the interactions of Ir(^{1}L)$_2$(^{2}L) molecules stacking along the crystal axes. The doped light-emitting diodes using this novel Ir(^{1}L)$_2$(^{2}L) complex as the phosphorescent dopant were fabricated. At a Ir(^{1}L)$_2$(^{2}L) concentration of 6.0 wt%, a green-yellow emitting OLED was achieved with a maximum external quantum efficiency (EQE) of 6.11% and a maximum luminous efficiency of 22.55 cd A^{-1} at the current density of 6.06 mA cm^{-2}, and a maximum luminance of 6653 cd m^{-2} at 10.7 V. Furthermore, two reference complexes Ir(^{1}L)$_2$(acac) and Ir(^{1}L)$_2$(TTA) were also used as emitters to fabricate OLED devices with the same device configuration. The maximum luminous efficiency of Ir(^{1}L)$_2$(acac) doped device was measured to be 20.04 cd A^{-1} at 2.15 mA cm^{-2} (10.0 wt%), while the doped device of Ir(^{1}L)$_2$(TTA) had a maximum luminous efficiency of 16.59 cd A^{-1} at 1.36 mA cm^{-2}. The better performances of Ir(^{1}L)$_2$(^{2}L) doped devices could be largely attributed to an improved hole-transporting property due to the introduction of the carbazole moiety.

Received 16th August 2013
Accepted 5th November 2013

DOI: 10.1039/c3ra44432e

www.rsc.org/advances

1. Introduction

Phosphorescent organic light-emitting diodes (PhOLEDs) have been intensively studied due to their high external quantum efficiencies.[1–7] Owing to the strong spin–orbital coupling of heavy-metal complexes, both singlet and triplet excitons can be harvested for light, and thus potentially 100% internal quantum efficiency can be obtained in PhOLEDs. The most well studied organometallic compounds are mainly complexes of noble metal ions such as Pt^{II},[1,8,9] Ir^{III},[2–7] Os^{II},[10,11] and Re^{I}.[12–14] Among organometallic compounds, cyclometalated iridium complexes are the most promising emitting materials due to their high quantum efficiency, brightness, color diversity and short excited-state lifetime. In order to develop the Ir(III) complex to possess wide range of phosphorescence color, high emission quantum yield and good stability, Ir(III) complexes with mixed ligands have been synthesized.[15,16] The photophysical properties and device performance parameters, such as the lowest unoccupied molecular orbital (LUMO) energy, the luminous efficiency and emission color of these Ir(III) complexes can be tuned by modifying the chemical structure of the cyclometalating ligands.[2,15,17–24] For example, Rehmann and co-workers[24] reported PhOLEDs fabricated with an iridium(III) complex of coumarin-6(iridium(III)bis(3-(2-benzothiazolyl)-7-(diethylamino)-coumarinato-N,C4′)(6-((3-ethyl-oxetan-3-yl)methoxy)hexylacetoacetate)) as the emitter, a maximum luminous efficiency of 18.4 cd A^{-1} and a power efficiency of 11.7 lm W^{-1} were achieved at 5 V and at a brightness of 100 cd m^{-2}.

Neutral homoleptic tris-cyclometalated Ir(C^N)$_3$ complexes based on 2-phenylpyridine (ppy) are one of the most popular and thoroughly studied green emissive iridium complexes.[25–27] Recently, we have reported three coumarin-based iridium(III) complexes,[28,29] in which 3-(pyridin-2-yl)coumarin was used as the cyclometalated ligand and acetylacetonate, thenoyltrifluoroacetonate and picolinate were used as the ancillary monoanionic ligand, respectively. These iridium complexes exhibit intensive green emissions, indicating that they are useful for the fabrication of organic light-emitting diodes.

[a]*Key Laboratory of Opto-Electronic Technology and Intelligent Control (Ministry of Education), Lanzhou Jiaotong University, Lanzhou 730070, P. R. China. E-mail: yutianzhi@hotmail.com; Fax: +86-931-4938756; Tel: +86-931-4956935*

[b]*College of Polymer Science and Polymer Engineering, The University of Akron, Ohio, 44325, USA. E-mail: scheng@uakron.edu; Fax: +330 972-8626; Tel: +330 972-6931*

[c]*Printable electronics research center, Suzhou Institute of Nano-Tech and Nano-Bionics, Chinese Academy of Sciences, Suzhou 215123, China*

† Electronic supplementary information (ESI) available: The structure determination of Ir(^{1}L)$_2$(^{2}L) crystal is described detailedly. Table S1 and Fig. S1–S4 are also given. See DOI: 10.1039/c3ra44432e

‡ These authors are contributed equally.

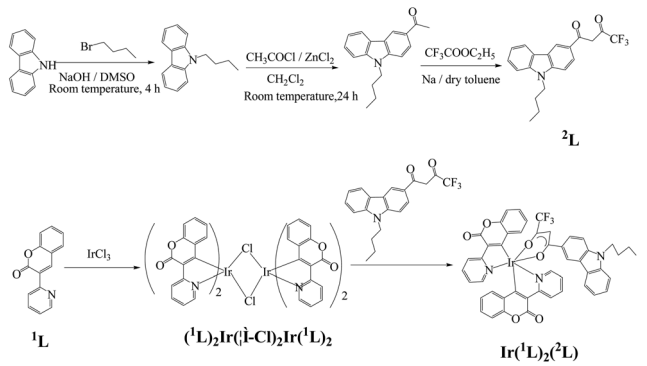

Scheme 1 Synthetic routes of ^{2}L and Ir(^{1}L)$_2$(^{2}L).

In this work, a new coumarin-based iridium(III) complex, Ir(^{1}L)$_2$(^{2}L), where ^{1}L is 3-(pyridin-2-yl)coumarinato, ^{2}L is 1-(9-butyl-9*H*-carbazol-3-yl)-4,4,4-trifluoro-butane-1,3-dionato, was designed and synthesized to study the effect of the improved hole-transporting property of the complex by modifying the β-diketonate ligand. The PhOLEDs fabricated with Ir(^{1}L)$_2$(^{2}L) as an emitter exhibited a maximum external quantum efficiency (EQE) of 6.11% and a maximum luminous efficiency of 22.55 cd A^{-1} at the current density of 6.06 mA cm^{-2}. The synthetic routes of the ancillary ligand (^{2}L) and Ir(^{1}L)$_2$(^{2}L) were shown in Scheme 1.

2. Experimental section

2.1 Materials and methods

Carbazole was purchased from Tianjin Guangfu Fine Chemical Research Institute (China) and recrystallized from methanol before use. *n*-Butyl bromide was obtained from Tanjing Kaixin Chemical Co. Ltd. (China). Ethyl trifluoroacetate and acetyl chloride were purchased from Aladdin Reagent Inc. and Alfa Aesar China Co. Ltd, respectively. 4,4′-Bis(9-carbazolyl)biphenyl (CBP), 4,4′,4″-tris(*N*-3-methylphenyl-*N*-phenylamino)triphenylamine (*m*-MTDATA), 1,3,5-tris(*N*-phenylbenzimidazol-2-yl)benzene (TPBi) and *N*,*N*′-bis-(naphthyl)-*N*,*N*′-diphenyl-1,1′-biphenyl-4,4′-diamine (NPB) were purchased from Electro-Light Technology Corp., Beijing. Other solvents were analytical reagents.

The cyclometalated coumarin ligand (3-(pyridine-2-yl) coumarin, ^{1}L) and cyclometalated Ir(III)μ-chlorobridged dimmer ((^{1}L)$_2$Ir(μ-Cl)$_2$Ir(^{1}L)$_2$) were prepared as previously described.[25,26]

IR spectra (400–4000 cm^{-1}) were carried out using a Shimadzu IRPrestige-21 FT-IR spectrophotometer. ^{1}H NMR spectra were obtained on Unity Varian-500 MHz. Elemental analyses were obtained using an Elemental Vario-EL automatic elemental analysis instrument. Melting points were measured by using an X-4 microscopic melting point apparatus (Beijing Taike Instrument Limited Company). UV-vis absorption and photoluminescent spectra were recorded on a Shimadzu UV-2550 spectrometer and on a Perkin-Elmer LS-55 spectrometer, respectively. The electroluminescent spectra were measured on a PR-650 SpectraScan Colorimeter.

The WAXD/TEM samples were prepared by casting a drop of Ir(^{1}L)$_2$(^{2}L) solution in chloroform (0.01 wt%) onto carbon coated mica sheet, which was placed in a tetrahydrofuran atmosphere. The single crystals of Ir(^{1}L)$_2$(^{2}L) were gradually grown within several hours under the tetrahydrofuran vapor. The mica sheet was immersed into water and the carbon film was floated onto the water, which was picked up onto copper grids for TEM characterization.

One-dimensional WAXD experiments were carried out on a Rigaku MultiFlex 2 kW tube-anode X-ray with a scanning rate of 1° min^{-1} at room temperature. The silicon powder was used to calibrate the peak postions in the high-angle region (>15°) and silver behenate in the low-angle region (<15°).

2.2 Synthesis and characterization of the Ir(III) complex (Ir(^{1}L)$_2$(^{2}L))

2.2.1 1-(9-Butyl-9*H*-carbazol-3-yl)-4,4,4-trifluorobutane-1,3-dione (^{2}L)

9-Butylcarbazole. A mixture of carbazole (4.00 g, 23.9 mmol), *n*-butyl bromide (3.27 g, 23.9 mmol) and sodium hydroxide (27.50 g, 687.5 mmol) in dimethyl sulfoxide (60 mL) was stirred in a 250 mL three-necked flask for 4 h at room temperature. The mixture was then poured into water, and extracted with ether (3 × 100 mL). The combined organic phase was washed with water (2 × 100 mL) and dried over anhydrous magnesium sulfate. After filtration and evaporation of the solvent, the crude product was purified by silica column chromatography with petroleum ether as the eluent to give 9-butylcarbazole (4.86 g, 91%). m.p. 58–59 °C. ^{1}H NMR ($CDCl_3$, δ, ppm): 8.10–8.08 (d, J = 7.6 Hz, 2H), 7.47–7.43 (m, 2H), 7.40–7.38 (d, J = 8.0 Hz, 2H), 7.24–7.20 (m, 2H), 4.31–4.27 (t, J = 7.2 Hz, 2H), 1.88–1.81 (m, 2H), 1.44–1.36 (m, 2H), 0.95–0.92 (t, J = 7.2 Hz, 3H).

3-Acetyl-9-butylcarbazole. To a solution of 9-butylcarbazole (4.78 g, 21.4 mmol) in dichloromethane (30 mL), anhydrous $ZnCl_2$ (4.38 g, 32.14 mmol) was added quickly. The mixture was stirred, and then a solution of acetyl chloride (2.52 mL, 32.1 mmol) in dichloromethane (15 mL) was added dropwise. The reaction mixture was stirred at room temperature for about 24 h, and then cooled water (100 mL) was added to the mixture. The product was extracted with dichloromethane (3 × 100 mL). The combined organic phase was washed with water (2 × 100 mL) and dried over anhydrous magnesium sulfate. After filtration and evaporation of the solvent, the crude product was purified by silica column chromatography with a mixture of ethyl acetate–petroleum ether (1 : 10) as eluent to afford 3-acetyl-9-butylcarbazole as a primrose yellow oil (4.71 g, 83%). ^{1}H NMR ($CDCl_3$, δ, ppm): 8.74 (d, J = 1.6 Hz, 1H), 8.16–8.10 (m, 2H), 7.53–7.49 (m, 1H), 7.44–7.38 (q, J = 8.0 Hz, 2H), 7.31–7.25 (q, J = 7.6 Hz, 1H), 4.33–4.29 (t, J = 7.2 Hz, 2H), 2.72 (s, 3H), 1.87–1.82 (q, J = 7.6 Hz, 2H), 1.42–1.36 (q, J = 7.2 Hz, 2H), 0.96–0.93 (t, J = 7.2 Hz, 3H).

1-(9-Butyl-9H-carbazol-3-yl)-4,4,4-trifluorobutane-1,3-dione (^{2}L). A suspension of fresh sodium (0.356 g, 15.5 mmol) in anhydrous toluene (30 mL) was placed in a three-necked flask. The mixture was heated up to 120 °C and stirred vigorously till the sodium was molten and scattered, then ethyl trifluoroacetate (2.20 g, 15.5 mmol) was added into the mixture. Meanwhile, a solution of 3-acetyl-9-butylcarbazole (4.107 g, 15.5 mmol) in toluene

(15 mL) was added dropwise. The reaction mixture was stirred at 120 °C for about 24 h. The mixture was poured into cooled water (100 mL), and then acidified with dilute hydrochloric acid to pH = 3. The mixture was extracted with $CHCl_3$ (3 × 100 mL), and the combined organic phase was dried over anhydrous $MgSO_4$. The solvent was removed under reduced pressure and the residue was purified by column chromatography on silica gel with a mixture of ethyl acetate–petroleum ether (1 : 15) as eluent to obtain 1-(9-butyl-9*H*-carbazol-3-yl)-4,4,4-trifluorobutane-1,3-dione as a yellow oil (3.21 g, 57.4%). ^{1}H NMR ($CDCl_3$, δ, ppm): 8.74–8.73 (d, J = 1.6 Hz, 1H), 8.18–8.16 (d, J = 8.0 Hz, 1H), 8.08–8.06 (q, J = 7.2 Hz, 1H), 7.56–7.52 (t, J = 7.2 Hz, 1H), 7.47–7.43 (t, J = 6.4 Hz, 2H), 7.35–7.32 (t, J = 7.2 Hz, 1H), 6.71 (s, 2H), 4.36–4.32 (t, J = 7.2 Hz, 2H), 1.92–1.88 (m, 2H), 1.44–1.36 (m, 2H), 0.99–0.93 (m, 3H).

2.2.2 Ir(III)bis(3-(pyridin-2-yl)coumarinato-N,C^4)(1-(9-butyl-9*H*-carbazol-3-yl)-4,4,4-trifluoro-butane-1,3-dionato-*O*,*O*) (Ir(^{1}L)$_2$(^{2}L)). The chloro-bridged dimer complex ((^{1}L)$_2$Ir(μ-Cl)$_2$Ir(^{1}L)$_2$) (0.200 g, 0.149 mmol), 1-(9-butyl-9*H*-carbazol-3-yl)-4,4,4-trifluorobutane-1,3-dione (0.269 g, 0.744 mmol) and sodium carbonate (0.710 g, 6.70 mmol) were refluxed in dichloroethane under nitrogen atmosphere for 12 h. After cooling, a small quantity of water was added. The mixture was extracted with dichloromethane (3 × 50 mL). The organic phase was washed with water (2 × 50 mL) and dried over anhydrous $MgSO_4$. After filtering, the filtrate was evaporated to dryness under reduced pressure. The crude was purified by chromatography on silica gel using ethyl acetate–petroleum ether (1 : 6, v/v) as the eluent to give Ir(^{1}L)$_2$(^{2}L) as a yellow powder (0.11 g, 71%). ^{1}H NMR($CDCl_3$, δ, ppm): 9.19 (t, 2H, J = 8.8, aryl–H), 8.45 (d, 1H, J = 1.6, aryl–H), 8.15–8.10 (m, 2H, aryl–H), 8.04 (d, 1H, J = 5.2, aryl–H), 7.95–7.82 (m, 3H, aryl–H), 7.51 (t, 1H, aryl–H), 7.42 (d, 1H, aryl–H), 7.35–7.23 (m, 6H, aryl–H), 7.10–7.06 (m, 1H, aryl–H), 7.01–6.97 (m, 1H, aryl–H), 6.71–6.66 (m, 2H, aryl–H), 6.39 (s, 1H, aryl–H), 6.25–6.17 (m, 2H, aryl–H), 4.29 (t, 2H, J = 6.8, N–CH_2–), 1.83 (t, 2H, J = 7.6, –CH_2–), 1.43–1.35 (m, 2H, –CH_2–), 0.93 (t, 3H, J = 7.2, –CH_3). ^{13}C NMR ($CDCl_3$, δ, ppm): 184.34, 181.44, 165.75, 156.80, 150.88, 147.89, 143.14, 141.07, 139.04, 132.02, 130.87, 128.88, 127.99, 126.64, 125.64, 123.77, 122.74, 121.13, 120.91, 120.73, 120.20, 116.30, 109.23, 108.83, 91.96, 76.99, 43.09, 30.96, 20.46, 13.80. Anal. calc. for $C_{48}H_{33}F_3IrN_3O_6$ (%): C, 57.82; H, 3.34; N, 4.21. Found: C, 58.03; H, 3.29; N, 4.32. MS (MALDI-TOF): m/z 1020.2 $[M + Na]^+$.

2.3 PhOLEDs fabrication and characterization

The multilayer PhOLEDs with a device architecture of ITO/*m*-MTDATA (10 nm)/NPB (20 nm)/CBP:complex (x wt%, 30 nm)/TPBi (30 nm)/LiF (1 nm)/Al (100 nm) were fabricated by vacuum-deposition method. All organic layers were sequentially deposited without breaking vacuum (2 × 10^{-5} Pa). Thermal deposition rates for organic materials, LiF and Al were ~2 Å s^{-1}, ~1 Å s^{-1} and 10 Å s^{-1}, respectively. The active area of the devices was 12 mm^2. The EL spectra and Commission Internationale de L'Eclairage (CIE) coordinates were measured on a Hitachi MPF-4 fluorescence spectrometer. The characterization of brightness–current–voltage (*B*–*I*–*V*) were measured with a 3645 DC power supply combined with a 1980A spot photometer and were recorded simultaneously. All measurements were done in the air at room temperature without any encapsulation.

3. Results and discussion

3.1 Molecular design and synthesis of Ir(^{1}L)$_2$(^{2}L)

The chemical structure of Ir(^{1}L)$_2$(^{2}L) is shown in Fig. 1a and the molecular model of Ir(^{1}L)$_2$(^{2}L) is shown in Fig. 1b with carbon, oxygen, nitrogen, iridium and fluorine atoms shown as purple, red, blue, orange and yellow balls, respectively. Based on the model established, the length of Ir(^{1}L)$_2$(^{2}L) along the molecular long *a* axis is about 2.0 nm and the width of Ir(^{1}L)$_2$(^{2}L) along the molecular short *b* axis that is perpendicular to the long axis is ~1.0 nm.

The cyclometalating ligand ^{1}L and the complexes Ir(^{1}L)$_2$(acac) and Ir(^{1}L)$_2$(TTA) were synthesized according to the procedure previously reported.[29] The synthetic route of the ancillary ligand ^{2}L and the complex Ir(^{1}L)$_2$(^{2}L) is shown in Scheme 1.

3.2 Ir(^{1}L)$_2$(^{2}L) single crystal morphology and structure determination

Fig. 2 shows a 1D WAXD power pattern of Ir(^{1}L)$_2$(^{2}L). The *d*-spacings of the first five strong diffraction peaks are 2.01 nm (2θ = 4.44°), 1.43 nm (2θ = 6.19°), 1.00 nm (2θ = 8.79°), 0.84 nm (2θ = 10.57°), and 0.74 nm (2θ = 11.90°), respectively. The *d*-spacing values of the first and third diffraction peaks are consistent with the length and width of Ir(^{1}L)$_2$(^{2}L) molecule, respectively, which are estimated based on the molecular

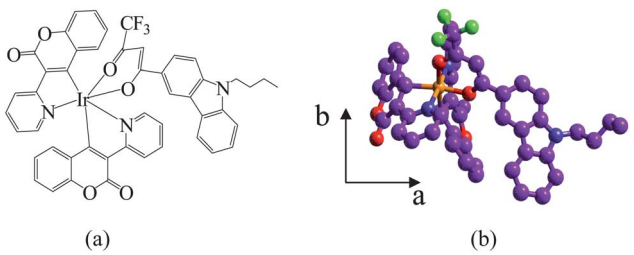

Fig. 1 Chemical structure (a) and molecular model (b) of Ir(^{1}L)$_2$(^{2}L).

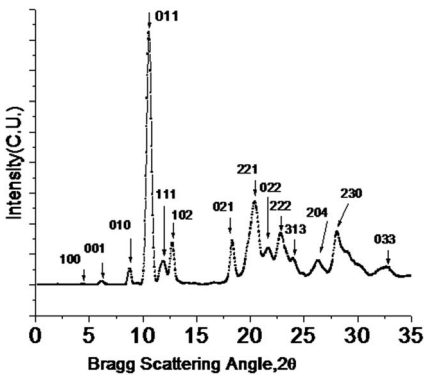

Fig. 2 One dimension wide X-ray diffraction pattern of Ir(^{1}L)$_2$(^{2}L).

model shown in Fig. 1b. Fig. 3a is a bright field TEM image of one elongated ribbon-like $Ir(^1L)_2(^2L)$ single crystal. Fig. 3b is a SAED pattern with the [001] zone taken from the crystal in Fig. 3a.

Combining the *d*-spacing calculations of the WAXD pattern and the crystal tilting experiments of TEM, the unit cell parameter of $Ir(^1L)_2(^2L)$ crystal can be determined to be $a = 2.03$ nm, $b = 0.99$ nm, $c = 1.49$ nm, $\alpha = \beta = \gamma = 90°$. The space group is assigned to be P_{222} by the international crystallographic table due to no extinction ED spots found in Fig. S1a–S1f (see ESI†). There are two $Ir(^1L)_2(^2L)$ molecules in one unit cell. The unit cell parameters are calculated in the Cerius[2] molecular package, and the preliminary packing model of $Ir(^1L)_2(^2L)$ single crystal is established along three crystal axes as shown in Fig. 4a–c. The calculated density ($d_{cal.} = 1.108$ g cm^{-3}) based on the unit cell parameters is found in accordance with the experimental data ($d_{mea.} = 1.102$ g cm^{-3}).

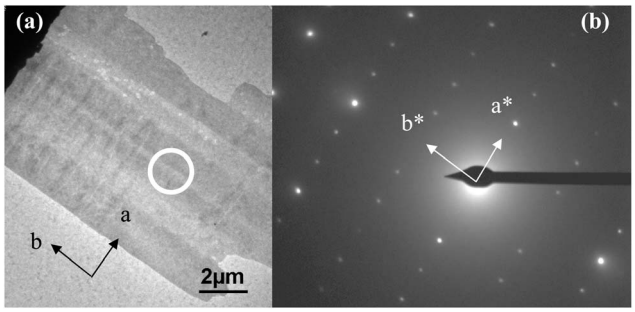

Fig. 3 (a) TEM bright filed morphology of the $Ir(^1L)_2(^2L)$ single crystal grown at room temperature by chloroform solution evaporation under tetrahydrofuran atmosphere. (b) A [001] zone-SAED pattern corresponding to the crystal within the circle area in (a).

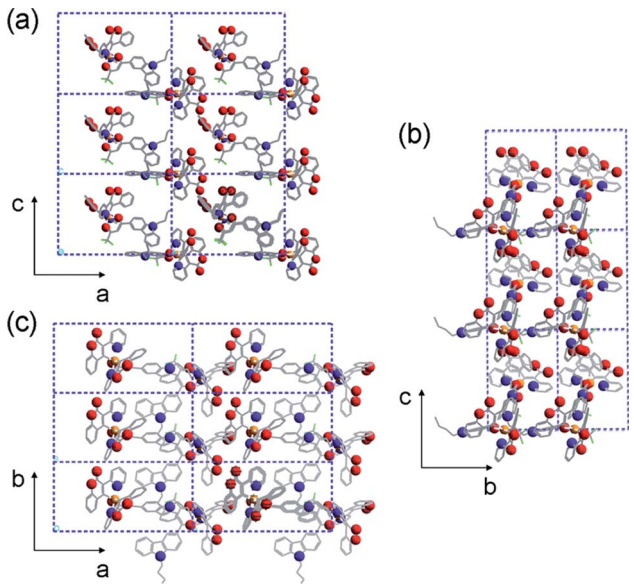

Fig. 4 Molecular packing model of $Ir(^1L)_2(^2L)$ single crystal established by Cerius[2] modeling package (a) *ac*-plane projection; (b) *bc*-plane projection; (c) *ab*-plane projection.

3.3 UV-vis absorption and photoluminescence spectra

The UV-vis absorption and photoluminescence spectra of $Ir(^1L)_2(^2L)$, $Ir(^1L)_2$(acac) and $Ir(^1L)_2$(TTA) were measured in diluted dichloromethane solutions at room temperature, as presented in Fig. 5. In UV-vis absorption spectrum of $Ir(^1L)_2(^2L)$, there are eight major absorptions at 213, 240, 276, 288, 348, 383, 405 and 436 nm, in which the absorption bands below 383 nm could be attributed to spin-allowed $\pi \rightarrow \pi^*$ transition of the ligands and the band around 383 nm can be assigned to the spin-allowed metal-to-ligand charge transfer ^{1}(MLCT) (metal–ligand-charge-transfer), and the bands at the longer wavelengths (405 and 436 nm) can be assigned to both spin–orbit coupling enhanced $^3(\pi \rightarrow \pi^*)$ and spin-forbidden ^{3}MLCT transitions.[30–32]

The absorption spectra of the complexes $Ir(^1L)_2$(acac) and $Ir(^1L)_2$(TTA) strongly resemble each other,[29] indicating that the absorption spectra are mainly decided by the ^{1}L ligand, and that the ancillary ligands, acetylacetone and thenoyltrifluoroaceton, scarcely play a role in the absorptions in the complexes compared with the absorption of ^{1}L ligand.[28] The stronger absorption bands at 200–350 nm can be assigned to the spin-allowed $^1(\pi \rightarrow \pi^*)$ transitions of the cyclometalated coumarin ligand ^{1}L in the complexes. The weak absorption bands (at 377, 409 and 433 nm for $Ir(^1L)_2$(TTA) and at 385, 419 and 439 nm for $Ir(^1L)_2$(acac)) can be ascribed to the admixture of ^{1}MLCT, ^{3}MLCT and $^3(\pi \rightarrow \pi^*)$ states.

Based on Fig. 5, the photoluminescence spectra of the complexes $Ir(^1L)_2(^2L)$, $Ir(^1L)_2$(acac) and $Ir(^1L)_2$(TTA) in dichloromethane solutions greatly resemble each other, all of which exhibit green emissions with a maximum main peak and a shoulder peak. But the photoluminescence spectrum of complex $Ir(^1L)_2(^2L)$ ($\lambda_{max} = 531$ nm, $\lambda_{min} = 568$ nm) shows a blue shift of 2 nm in comparison with that of complexes $Ir(^1L)_2$(acac) and $Ir(^1L)_2$(TTA) ($\lambda_{max} = 533$ nm, $\lambda_{min} = 570$ nm) due to lower ligand-field strength of ligand ^{1}L anion than acac and TTA anions.[15,33]

The quantum yields of the complexes $Ir(^1L)_2(^2L)$, $Ir(^1L)_2$(acac) and $Ir(^1L)_2$(TTA) at room temperature were measured to be

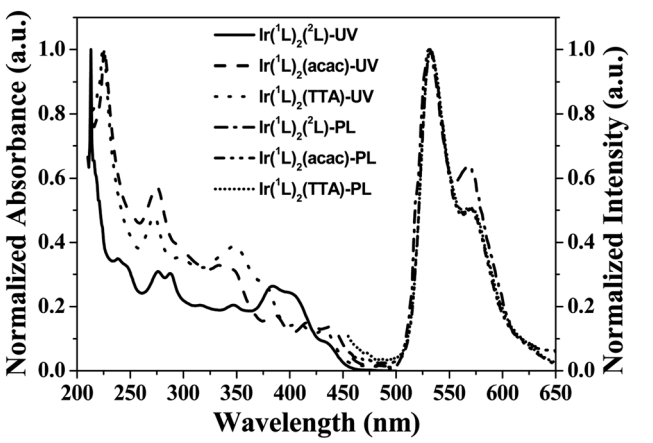

Fig. 5 Normalized UV-vis absorption and photoluminescence spectra of $Ir(^1L)_2(^2L)$, $Ir(^1L)_2$(acac) and $Ir(^1L)_2$(TTA) in diluted dichloromethane solutions ($C = 1 \times 10^{-6}$ mol L^{-1}).

10.36%, 9.15% and 9.08% from the THF solutions (*ca.* 10^{-6} mol L^{-1}) by an absolute method using the Edinburgh Instruments (FLS920) integrating sphere excited at 380 nm with the Xe lamp. The lifetime decays of the complexes $Ir(^1L)_2(^2L)$, $Ir(^1L)_2$(acac) and $Ir(^1L)_2$(TTA) were measured to be ($\tau_1 = 0.72$ μs, $\tau_1 = 9.05$ μs), ($\tau_1 = 0.79$ μs, $\tau_1 = 9.22$ μs) and ($\tau_1 = 0.81$ μs, $\tau_1 = 9.27$ μs) by a time-correlated single photon counting spectrometer using Edinburgh Instruments (FLS920) with a microsecond flashlamp as the excitation source (repetition rate 90 Hz) at room temperature.

3.4 LUMO and HOMO energy levels of $Ir(^1L)_2(^2L)$ by cyclic voltammetry measurement

The LUMO and HOMO energy levels of $Ir(^1L)_2(^2L)$ were calculated from cyclic voltammetry (CV) measurement and absorption spectrum. $Ir(^1L)_2(^2L)$ was dissolved in dichloromethane with tetra-*n*-butylammonium tetrafluoroborate (0.1 mol L^{-1}) as the electrolyte. A platinum working electrode and a saturated Ag/AgCl reference electrode were used. Ferrocene was used for potential calibration. Fig. S3† shows the cyclic voltammogram of $Ir(^1L)_2(^2L)$, from which the oxidation onset at 0.81 V was clearly observed. At the same condition, the oxidation peak and the reductive peak were observed at 0.55 and 0.25 V, respectively, then the $E_{1/2}$ (Fc/Fc^+) is 0.40 V. Thus the HOMO energy level of $Ir(^1L)_2(^2L)$ was determined to be −5.21 eV regarding the energy level of ferrocene/ferrocenium as −4.80 eV. The optical band gap of $Ir(^1L)_2(^2L)$ was estimated to be 461 nm, which corresponds to 2.69 eV. Then the LUMO of $Ir(^1L)_2(^2L)$ is calculated to be −2.52 eV.

On the basis of the oxidation potentials together with the extrapolated absorption edge data of $Ir(^1L)_2$(acac) and $Ir(^1L)_2$(TTA), their HOMO and LUMO energy levels can similarly be estimated. For $Ir(^1L)_2$(acac), the determined HOMO and LUMO energy levels are −5.28 eV and 2.61 eV, while for $Ir(^1L)_2$(TTA), the results are −5.30 eV and −2.59 eV.

3.5 PhOLEDs performance

The devices with a configuration of ITO/*m*-MTDATA (10 nm)/NPB (20 nm)/CBP:complex (*x* wt%, 30 nm)/TPBi (30 nm)/LiF (1 nm)/Al (100 nm) were fabricated. The diagram of HOMO and LUMO energy levels of the materials are depicted in Fig. 6. The emitting layers are consisted of host materials CBP and dopants of the complexes $Ir(^1L)_2(^2L)$ or $Ir(^1L)_2$(acac) or $Ir(^1L)_2$(TTA) at different concentrations (*x* wt%). *m*-MTDATA, NPB and TPBi were used as hole injection, hole transport and electron transport materials, respectively. LiF was used as the electron-injection layer.

From the energy diagram, strong hole trapping can be expected due to the lower HOMO levels of the complexes than that of CBP. On the other hand, little variation in LUMO level between the complex and CBP allows the electron to be injected into the complex easily. Moreover, it is clear that NPB and TPBi can act as substantial electron-blocking and hole-blocking layers, respectively. As a result, effective electron–hole pair confinement in the emission layer can be expected.

The electroluminescence (EL) spectra of PhOLEDs are shown in Fig. S4.† From Fig. S4a,† when the doping concentration of $Ir(^1L)_2(^2L)$ is 6 wt%, the shape of EL spectra did not change at different applied voltages. The EL spectra of $Ir(^1L)_2(^2L)$ resemble closely its PL spectrum in thin film with a maximum main peak at 531 nm and a shoulder peak at 570 nm. It can be seen that the EL spectra of devices with different doping concentrations of $Ir(^1L)_2$(acac) and $Ir(^1L)_2$(TTA) also did not change and resemble closely their respective PL spectra in thin films (Fig. S4b and

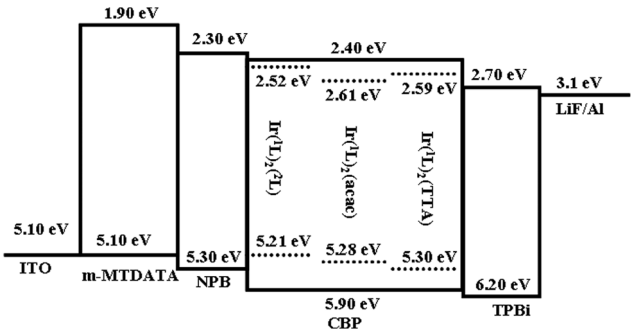

Fig. 6 Energy-level diagram of the materials in the device. Device configuration: ITO/*m*-MTDATA/NPB/CBP:complex (*x* wt%)/TPBi/LiF/Al.

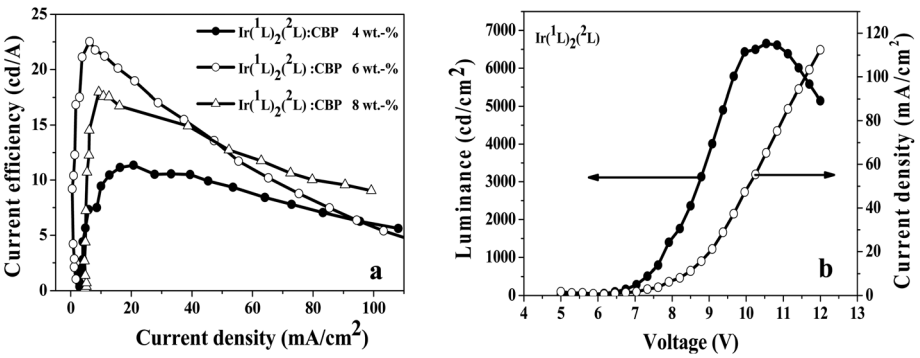

Fig. 7 (a) Current efficiency *vs.* current density characteristics of the devices at various $Ir(^1L)_2(^2L)$ doping concentrations; (b) current density–luminance–voltage characteristics of the device at 6.0 wt% $Ir(^1L)_2(^2L)$ doping concentration. Device configuration: ITO/*m*-MTDATA/NPB/CBP:complex (*x* wt%)/TPBi/LiF/Al.

Table 1 EL performances of the $Ir(^1L)_2(^2L)$ doped devices

Entry	V_{on} (V)	L_{max} (cd m^{-2})	LE_{max} (cd A^{-1})	LE (20 mA cm^{-2})	EQE_{max} (%)	$CIE_{x,y}$
4.0 wt%	6.3	6066	11.40 @ 20.0 mA cm^{-2}	11.40	3.09%	(0.473, 0.507)
6.0 wt%	6.4	6653	22.55 @ 6.06 mA cm^{-2}	19.22	6.11%	(0.479, 0.510)
8.0 wt%	6.6	8972	18.00 @ 9.32 mA cm^{-2}	16.46	4.88%	(0.481, 0.504)

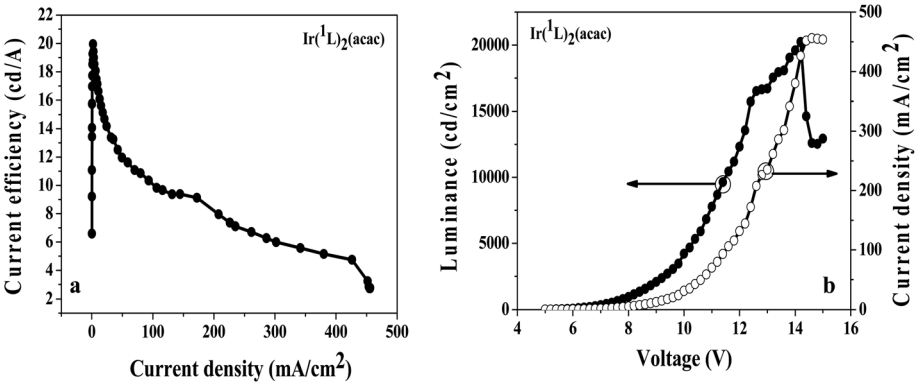

Fig. 8 (a) Current efficiency *vs.* current density characteristics and (b) current density–luminance–voltage characteristics of the device at 10.0 wt % $Ir(^1L)_2$(acac) doping concentration. Device configuration: ITO/*m*-MTDATA/NPB/CBP:complex (*x* wt%)/TPBi/LiF/Al.

S4c†). It was also found that the EL spectra of PhOLEDs incorporated with the complexes $Ir(^1L)_2(^2L)$ and $Ir(^1L)_2$(acac) and $Ir(^1L)_2$(TTA) were independent of the applied voltages and doping concentrations of $Ir(^1L)_2(^2L)$ and $Ir(^1L)_2$(acac) and $Ir(^1L)_2$(TTA).

Fig. 7a shows the relationship between luminous efficiency and the current density in PhOLEDs fabricated with different $Ir(^1L)_2(^2L)$ doping concentrations. It was found that all PhOLEDs have higher luminous efficiencies at low current densities, and then the luminous efficiencies fall off at higher current densities. Table 1 summarized the performances of PhOLEDs with various $Ir(^1L)_2(^2L)$ doping concentrations in CBP host. The turn-on voltages (V_{on}) of the devices are between 6.3 V and 6.6 V, and the brightness is between 6066 cd m^{-2} and 8972 cd m^{-2}. By comparing the performance of different doping concentrations, the 6.0 wt% $Ir(^1L)_2(^2L)$ doped device has a maximum efficiency of 22.55 cd A^{-1} at 6.06 mA cm^{-2}, which has a green-yellow color with a CIE_{xy} of (0.479, 0.510). Even at 20 mA cm^{-2}, the doped device has a maximum efficiency of 19.22 cd A^{-1}. A maximum external quantum efficiency (EQE) of 6.11% was achieved. From the results, it is indicated that 6.0 wt% is the optimal doping concentration of $Ir(^1L)_2(^2L)$. The luminance and current density *vs.* voltage and current density *vs.* voltage characteristics of the devices at 6.0 wt% doping concentration are shown in Fig. 7b. The device shows a turn-on voltage of about 6.4 V, the maximum brightness is about 6653 cd m^{-2} at 10.7 V.

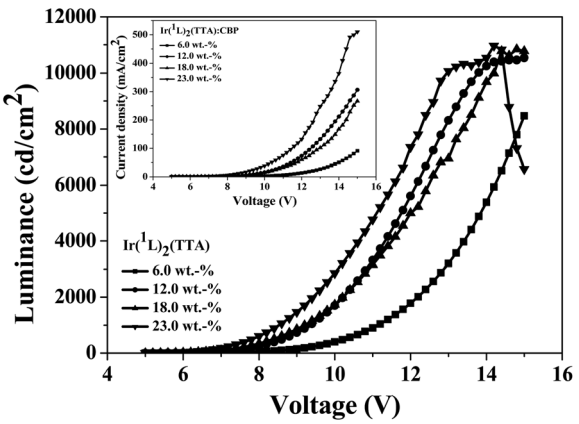

Fig. 9 Luminance and current density (inset) *vs.* voltage characteristics of the devices at various $Ir(^1L)_2$(TTA) doping concentrations. Device configuration: ITO/*m*-MTDATA/NPB/CBP:complex (*x* wt%)/TPBi/LiF/Al.

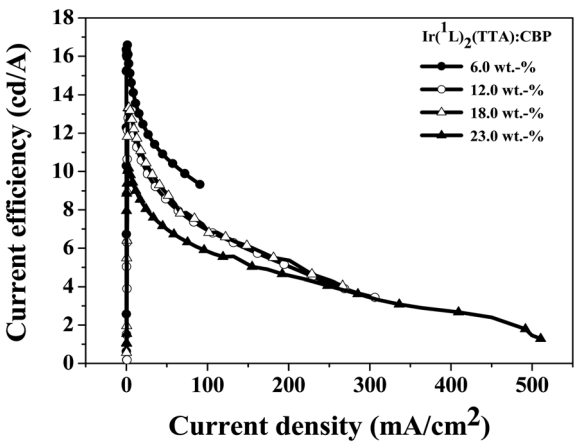

Fig. 10 Current efficiency *vs.* current density characteristics of the devices at various $Ir(^1L)_2$(TTA) doping concentrations. Device configuration: ITO/*m*-MTDATA/NPB/CBP:complex (*x* wt%)/TPBi/LiF/Al.

Table 2 EL performances of the $Ir(^1L)_2(TTA)$ doped devices

Entry	V_{on} (V)	L_{max} (cd m^{-2})	LE_{max} (cd A^{-1})	LE (20 mA cm^{-2})	EQE_{max} (%)	$CIE_{x,y}$
6.0 wt%	8.8	8470	16.59 @ 1.36 mA cm^{-2}	12.52	4.37%	(0.384, 0.592)
12.0 wt%	7.0	10 540	12.79 @ 2.44 mA cm^{-2}	10.47	3.48%	(0.400, 0.578)
18.0 wt%	6.8	10 840	13.35 @ 3.82 mA cm^{-2}	10.76	3.61%	(0.395, 0.581)
23.0 wt%	6.6	10 970	10.16 @ 3.01 mA cm^{-2}	8.39	2.78%	(0.402, 0.575)

In order to compare the electrophosphorescence performances of the $Ir(^1L)_2(^2L)$, the devices using $Ir(^1L)_2$(acac) and $Ir(^1L)_2$(TTA), respectively, as doped emitters were fabricated with the same device configuration of ITO/*m*-MTDATA/NPB/CBP:complex (*x* wt%)/TPBi/LiF/Al. For the complex $Ir(^1L)_2$(acac), the doped devices with different concentrations (6.0, 8.0, 10.0 and 12.0 wt%) were investigated, in which the 10.0 wt% doped device has a maximum efficiency. Thus, we chose 10.0 wt% as the optimal doping concentration of $Ir(^1L)_2$(acac). Fig. 8 displays the luminous efficiency *versus* the current density characteristics and the current density–luminance–voltage characteristics of PhOLEDs with 10.0 wt% $Ir(^1L)_2$(acac) doping concentrations, respectively. The turn-on voltage of these PhOLEDs is the same. It is at ~6.4 V, the maximum brightness is ~20 399 cd m^{-2} at 14 V, and the PhOLEDs exhibit a maximum luminous efficiency of 20.04 cd A^{-1} at 2.15 mA cm^{-2}, and a maximum external quantum efficiency (EQE) of 5.22%. The EL color of the PhOLEDs is green-yellow with a CIE_{xy} of (0.375, 0.599). The luminous efficiency declines relatively faster with the increase of current density at low current density (<100 mA cm^{-2}), this is probably attributed to the faster increase of triplet–triplet (T–T) annihilation and field-induced quenching effects.[33] At current density of 100 mA cm^{-2}, the luminous efficiency of the PhOLEDs reaches 14.88 cd A^{-1}.

Fig. 9 presents the current density and luminance *versus* bias voltage curves of the PhOLEDs fabricated with $Ir(^1L)_2$(TTA) at different doping concentrations 6.0, 12.0, 18.0 and 23 wt%. Fig. 10 shows the luminous efficiency *versus* current density characteristics of the PhOLEDs at various $Ir(^1L)_2$(TTA) doping concentrations. The CIE_{xy} color coordinates of the devices are near $x = 0.395$ and $y = 0.582$, which correspond to the green-yellow region of the CIE chromaticity diagram. The performance of 6.0 wt% doped device had a luminance of 8470 cd m^{-2} at 15 V and a maximum current efficiency of 16.59 at 1.36 mA cm^{-2} and a maximum external quantum efficiency (EQE) of 4.37%. As the doping concentration increased, the luminance of the devices increased from 10 540 to 10 970 cd m^{-2} and the current efficiency of the devices decreased. The EL performances of the $Ir(^1L)_2$(TTA) doped devices were given in Table 2.

Compared with the devices made from $Ir(^1L)_2$(acac) and $Ir(^1L)_2$(TTA), the devices made from $Ir(^1L)_2(^2L)$ have lower luminance, but they have higher current efficiencies. From the structures of the ancillary ligands (^2L, acac and TTA), the ligand ^2L has a bulky 9-butylcarbazole moiety which may be of benefit to the emitting center due to separating the emitting centers from each other and reducing the triplet–triplet annihilation to some extent. On the other hand, the carbazole-functionalized β-diketonate ^2L has preferable hole-transporting ability which is enlarged by π–π stacking of $Ir(^1L)_2(^2L)$ molecules shown in the $Ir(^1L)_2(^2L)$ crystal structure (Fig. 4). All these results demonstrated that the complex $Ir(^1L)_2(^2L)$ has a better hole-transporting property and a larger exciton recombination area than the complexes $Ir(^1L)_2$(acac) and $Ir(^1L)_2$(TTA) leading to the reduction of the triplet–triplet annihilation.[34] The results show that the complex $Ir(^1L)_2(^2L)$ is a better electroluminescent phosphor for OLEDs.

4. Conclusion

A novel iridium complex containing coumarin derivative as a cyclometalated ligand (^1L) and a carbazole-functionalized β-diketonate (^2L) as the ancillary ligand, $Ir(^1L)_2(^2L)$, were successfully synthesized and characterized. The crystal structure has been determined *via* combined WAXD and SAED experiments, and it is orthorhombic with a space group of P_{222}. The molecular packing model of $Ir(^1L)_2(^2L)$ single crystal shows that the π–π interaction favors the stacking of $Ir(^1L)_2(^2L)$ molecule in three dimensional space. This could form a channel for hole transportation which enhances the hole mobility. The PhOLEDs fabricated by the complex $Ir(^1L)_2(^2L)$ possess better performance as compared with those fabricated by similar complexes $Ir(^1L)_2$(acac) and $Ir(^1L)_2$(TTA). The better performance of $Ir(^1L)_2(^2L)$ is mainly attributed to the high PL quantum efficiency and low triplet–triplet (T–T) annihilation of $Ir(^1L)_2(^2L)$.

Acknowledgements

This work was supported by the National Natural Science Foundations of China (61166003 and 60776006), and the Program for Changjiang Scholars and Innovative Research Team in University (IRT0629). Also, it was supported by US NSF (DMR-0906898) and the Joint-Hope Education Foundation.

References

1 M. A. Baldo, D. F. O'Brien, Y. You, A. Shoustikov, S. Sibley, M. E. Thompson and S. R. Forrest, Highly efficient phosphorescent emission from organic electroluminescent devices, *Nature*, 1998, **395**, 151–154.

2 S. Lamansky, P. Djurovich, D. Murphy, F. Abdel-Razzaq, H. E. Lee, C. Adachi, P. E. Burrow, S. R. Forrest and M. E. Thompson, Highly phosphorescent bis-cyclometalated iridium complexes: synthesis, photophysical characterization, and use in organic light emitting diodes, *J. Am. Chem. Soc.*, 2001, **123**, 4304–4312.

3 X. Gong, M. R. Robinson, J. C. Ostrowski, D. Moses, G. C. Bazan and A. J. Heeger, High-efficiency polymer-based electrophosphorescent devices, *Adv. Mater.*, 2002, **14**, 581–585.

4 X. Gong, J. C. Ostrowski, G. C. Bazan, A. J. Heeger, M. S. Liu and A. K. Y. Jen, Electrophosphorescence from a conjugated copolymer doped with an iridium complex: high brightness and improved operational stability, *Adv. Mater.*, 2003, **15**, 45–49.

5 P. T. Chou and Y. Chi, Phosphorescent dyes for organic light-emitting diodes, *Chem.–Eur. J.*, 2007, **13**, 380–395.

6 M. S. Lowry and S. Bernhard, Synthetically tailored excited states: phosphorescent, cyclometalated iridium(III) complexes and their applications, *Chem.–Eur. J.*, 2006, **12**, 7970–7977.

7 W. S. Huang, C. W. Lin, J. T. Lin, J. S. Huang, C. W. Chu, Y. H. Wu and H. C. Lin, Highly branched green phosphorescent tris-cyclometalated iridium(III) complexes for solution-processed organic light-emitting diodes, *Org. Electron.*, 2009, **10**, 594–606.

8 M. Thompson, The evolution of organometallic complexes in organic light-emitting devices, *MRS Bull.*, 2007, **32**, 694–701.

9 R. C. Kwong, S. Sibley, T. Dubovoy, M. Baldo, S. R. Forrest and M. E. Thompson, Efficient, saturated red organic light emitting devices based on phosphorescent platinum(II) porphyrins, *Chem. Mater.*, 1999, **11**, 3709–3713.

10 X. Z. Jiang, A. K. Y. Jen, B. Carlson and L. R. Dalton, Red electrophosphorescence from osmium complexes, *Appl. Phys. Lett.*, 2002, **80**, 713–715.

11 J. H. Kim, M. S. Liu, A. K. Y. Jen, B. Carlson, L. R. Dalton, C. F. Shu and R. Dodda, Bright red-emitting electrophosphorescent device using osmium complex as a triplet emitter, *Appl. Phys. Lett.*, 2003, **83**, 776–778.

12 X. Gong, P. K. Ng and W. K. Chan, Trifunctional light-emitting molecules based on rhenium and ruthenium bipyridine complexes, *Adv. Mater.*, 1998, **10**, 1337–1340.

13 S. Ranjan, S. Y. Lin, K. C. Hwang, Y. Chi, W. L. Ching, C. S. Liu, Y. T. Tao, C. H. Chien, S. M. Peng and G. H. Lee, Realizing green phosphorescent light-emitting materials from rhenium(I) pyrazolato diimine complexes, *Inorg. Chem.*, 2003, **42**, 1248–1255.

14 Z. J. Si, J. Li, B. Li, F. F. Zhao, S. Y. Liu and W. L. Li, Synthesis, structural characterization, and electrophosphorescent properties of rhenium(I) complexes containing carrier-transporting groups, *Inorg. Chem.*, 2007, **46**, 6155–6163.

15 Y. You and S. Y. Park, Phosphorescent iridium(III) complexes: toward high phosphorescence quantum efficiency through ligand control, *Dalton Trans.*, 2009, 1267–1282.

16 L. X. Xiao, Z. J. Chen, B. Qu, J. X. Luo, S. Kong, Q. H. Gong and J. Kido, Recent progresses on materials for electrophosphorescent organic light-emitting devices, *Adv. Mater.*, 2011, **23**, 926–952.

17 S. Lamansky, P. Djurovich, D. Murphy, F. Abdel-Razzaq, R. Kwong, I. Tsyba, M. Bortz, B. Mui, R. Bau and M. E. Thompson, Synthesis and characterization of phosphorescent cyclometalated iridium complexes, *Inorg. Chem.*, 2001, **40**, 1704–1711.

18 Y. S. Park, J. W. Kang, D. M. Kang, J. W. Park, Y. H. Kim, S. K. Kwon and J. J. Kim, Efficient, color stable white organic light-emitting diode based on high energy level yellowish-green dopants, *Adv. Mater.*, 2008, **20**, 1957–1961.

19 R. Ragni, E. A. Plummer, K. Brunner, J. W. Hofstraat, F. Babudri, G. M. Farinola, F. Naso and L. De Cola, Blue emitting iridium complexes: synthesis, photophysics and phosphorescent devices, *J. Mater. Chem.*, 2006, **16**, 1161–1170.

20 Y. You and S. Y. Park, Inter-ligand energy transfer and related emirrion change in the cyclometalated heteroleptic iridium complex: facile and efficient color tuning over the whole visible range by the ancillary ligand structure, *J. Am. Chem. Soc.*, 2005, **127**, 12438–12439.

21 I. Avilow, P. Minoofar, J. Comil and L. De Cola, Influence of substituents on the energy and nature of the lowest excited states of heteroleptic phosphorescent Ir(III) complexes: A joint theoretical and experimental study, *J. Am. Chem. Soc.*, 2007, **129**, 8247–8258.

22 S. Stagni, S. Colella, A. Palazzi, G. Valenti, S. Zacchini, F. Paolucci, M. Marcaccio, R. Q. Albuquerque and L. De Cola, Essential role of the ancillary ligand in the color tuning of iridium tetrazolate complexes, *Inorg. Chem.*, 2008, **47**, 10509–10521.

23 K. Hanson, A. Tamayo, V. V. Diev, M. T. Whited, P. I. Djurovich and M. E. Thompson, Efficient dipyrrin-centered phosphorescence at room temperature from bis-cyclometalated iridium(III) dipyrrinato complexes, *Inorg. Chem.*, 2010, **49**, 6077–6084.

24 N. Rehmann, C. Ulbricht, A. Köhnen, P. Zacharias, M. C. Gather, D. Hertel, E. Holder, K. Meerholz and U. S. Schubert, Advanced device architecture for highly efficient organic light-emitting diodes with an orange-emitting crosslinkable iridium(III) complex, *Adv. Mater.*, 2008, **20**, 129–133.

25 M. Cai, Z. Ye, T. Xiao, R. Liu, Y. Chen, R. W. Mayer, R. Biswas, K. M. Ho, R. Shinar and J. Shinar, Extremely efficient indium-tin-oxide-free green phosphorescent organic light-emitting diodes, *Adv. Mater.*, 2012, **24**, 4337–4342.

26 M. Cai, T. Xiao, E. Hellerich, Y. Chen, R. Shinar and J. Shinar, Hight-efficiency solution-processed small molecule eletrophosphorescent organic light-emitting diodes, *Adv. Mater.*, 2011, **23**, 3590–3596.

27 D. Tanaka, H. Sasabe, Y. J. Li, S. J. Su, T. Takeda and J. Kido, Ultra high efficiency green organic light-emitting devices, *Jpn. J. Appl. Phys.*, 2007, **46**, L10–L12.

28 T. Z. Yu, S. D. Yang, Y. L. Zhao, H. Zhang, D. W. Fan, X. Q. Han and Z. M. Liu, Synthesis, crystal structure and photoluminescent property of an iridium complex with coumarin derivative ligand, *Inorg. Chim. Acta*, 2011, **379**, 171–174.

29 T. Z. Yu, S. D. Yang, J. Meng, Y. L. Zhao, H. Zhang, D. W. Fan, X. Q. Han and Z. M. Liu, Synthesis, Crystal Structure and Photoluminescence of Iridium(III) Coumarin Complexes, *Inorg. Chem. Commun.*, 2011, **14**, 159–161.

30 H. H. Rho, G. Y. Park, Y. Ha and Y. S. Kim, Synthesis and photophysical studies of iridium complexes having different ligands, *Jpn. J. Appl. Phys.*, 2006, **45**, 568–573.
31 Z. Bao, A. J. Lovinger and J. Brown, New air-stable *n*-channel organic thin film transistors, *J. Am. Chem. Soc.*, 1998, **120**, 207–208.
32 Y. Wang, N. Herron, V. V. Grushin, D. LeCloux and V. Petrov, Highly efficient electroluminescent materials based on fluorinated organometallic iridium compounds, *Appl. Phys. Lett.*, 2001, **79**, 449–451.
33 C.-L. Ho, W.-Y. Wong, G.-J. Zhou, B. Yao, Z. Y. Xie and L. X. Wang, Solution-processible multi-component cyclometalated iridium phosphors for high-efficiency orange-emitting OLEDs and their potential use as white light sources, *Adv. Funct. Mater.*, 2007, **17**, 2925–2936.
34 Z. W. Liu, M. Guan, Z. Q. Bian, D. B. Nie, Z. L. Gong, Z. B. Li and C. H. Huang, Red phosphorescent iridium complex containing carbazole-functionalized β-diketonate for highly efficient nondoped organic light-emitting diodes, *Adv. Funct. Mater.*, 2006, **16**, 1441–1448.

